

1 **Measurement of J/ψ polarization and spin alignment in**
2 **Ru+Ru and Zr+Zr collisions at $\sqrt{s_{NN}} = 200$ GeV at STAR**

3 **Dandan Shen and Qian Yang, for the STAR Collaboration**

4 *Shandong University,*
5 *72 Binhai Road, Jimo, Qingdao, P.R. China*
6 *E-mail: shendandan@mail.sdu.edu.cn*

The heavy quark pairs are produced early in heavy-ion collisions and experience the full evolution of the Quark-Gluon Plasma created in these collisions. J/ψ serves as one of the important probes to study the properties of the QGP. Using the high-statistics Ru+Ru and Zr+Zr collision data at $\sqrt{s_{NN}} = 200$ GeV recorded by the STAR experiment, it has been observed that the J/ψ yield is strongly suppressed and its elliptic flow is consistent with zero indicating color screening of the heavy quark-antiquark pair potential in the medium and its potentially small regeneration contribution, respectively. Besides those observables, the J/ψ polarization can shed new light on the QGP properties and the J/ψ production mechanism in heavy-ion collisions.

In these proceedings, we present the first measurement of J/ψ polarization in heavy-ion collisions at RHIC. The study is carried out by reconstructing the J/ψ through its di-electron decay channel at mid-rapidity ($|y| < 1$). The J/ψ polarization parameters are measured in the Helicity frame, Collins-Soper frame, and the spin alignment is extracted with respect to the event plane. We conclude by presenting the physics implications of this measurement.

25th International Spin Physics Symposium (SPIN 2023)
24-29 September 2023
Durham, NC, USA

8 1. Introduction

9 Particle polarization in heavy-ion collisions provides a new insight into the study of Quark-
10 Gluon Plasma (QGP) and has recently gained increasing attention [1]. In 2005, Z. Liang and X.
11 Wang introduced the concept of vector meson spin alignment in heavy-ion collisions [2], and the
12 STAR collaboration reported for the first time the global spin alignment of ϕ meson [3]. Compared
13 to strange quarks, charm quarks are produced early in heavy-ion collisions, allowing them to
14 experience the full evolution of QGP. Therefore, the polarization of J/ψ may be influenced by the
15 medium effects in heavy-ion collisions [4].

16 The polarization of J/ψ meson serves as a valuable tool for investigating the production
17 mechanism in proton+proton ($p+p$) collisions [5]. Various models, such as the Colour-Singlet
18 Model (CSM), Non-Relativistic QCD (NRQCD) approach, and Improved Color Evaporation Model,
19 predict different polarization values and dependencies on transverse momentum (p_T) [6]. However,
20 the interpretation of the J/ψ polarization measurement is more complex due to the feed-down
21 contribution, which accounts for about 40% of the observed J/ψ yield, and it contributes to the
22 J/ψ polarization [4]. To date, no significant polarization for inclusive J/ψ has been observed in
23 $p+p$ collisions at RHIC and LHC energies [5, 7–10].

24 The QGP could affect J/ψ polarization in heavy-ion collisions. In addition, the inclusive J/ψ
25 production may differ between heavy-ion and proton-proton collisions due to modifications in the
26 feed-down of J/ψ originating from suppressed $\psi(2S)$ and χ_c states in the QGP [4]. This sequential
27 melting of charmonium states has been observed at LHC energy [11] and also recently in Ru+Ru and
28 Zr+Zr collisions at the STAR experiment, confirming the stronger suppression of $\psi(2S)$ compared
29 to J/ψ . The J/ψ polarization has been previously measured in Pb+Pb collisions at $\sqrt{s_{\text{NN}}} = 5.02$
30 TeV [12], and we may expect different polarization results at the RHIC energy due to the different
31 production mechanisms between the LHC and RHIC energies. Furthermore, a model predicts a
32 low- p_T polarization of J/ψ meson, between 0.35 and 0.4 in the Helicity frame (HX) for heavy-ion
33 collisions at RHIC energy if nonperturbative QCD effects are screened by the QGP [4]. On the
34 other hand, the J/ψ could also be produced through the charm and anti-charm coalescence process,
35 similar to the production of the ϕ meson in QGP. In this case, the coalesced J/ψ mesons could also
36 exhibit a global spin alignment behavior. At the LHC energies, there is a significant coalescence
37 contribution to the final J/ψ meson production, and ALICE has measured a J/ψ spin alignment
38 (ρ_{00}) of less than 1/3 in the forward rapidity region [13].

39 Measuring the polarization of J/ψ mesons in heavy-ion collisions serves as a promising probe
40 for studying the QGP. The production via coalescence of J/ψ only plays a partial role in the
41 observed J/ψ meson production in Ru+Ru and Zr+Zr collisions at the top RHIC energy, primarily
42 due to smaller system size and lower collisions energy. Measuring the J/ψ spin alignment at RHIC,
43 which has different collision energy and rapidity coverage compared to the LHC, provides a unique
44 opportunity to study the polarization of primordially produced J/ψ mesons after undergoing QGP
45 evolution. In these proceedings, the results on J/ψ polarization and spin alignment in Ru+Ru and
46 Zr+Zr collisions at $\sqrt{s_{\text{NN}}} = 200$ GeV at RHIC are reported.

47 2. Analysis Methodology

48 The polarization of the J/ψ state in dilepton decay channel is reflected in the geometrical shape
 49 of the angular distribution of the two decay products, which can be expressed using three parameters
 50 λ_θ , λ_ϕ and $\lambda_{\theta\phi}$ as described by the equation: [6]

$$W(\cos\theta, \phi) \propto \frac{1}{3 + \lambda_\theta} (1 + \lambda_\theta \cos^2\theta + \lambda_\phi \sin^2\theta \cos 2\phi + \lambda_{\theta\phi} \sin 2\theta \cos\phi), \quad (1)$$

51 where θ and ϕ are the polar and azimuthal angles of the positively charged daughter lepton in the
 52 J/ψ rest frame with respect to a chosen quantization axis (z-axis). The analysis involves the selection
 53 of three distinct reference systems for determining angular variables: the HX and the Collins-Soper
 54 frame (CS) with respect to the production plane, and the Event Plane frame (EP) with respect to
 55 the second order event-plane [1]. In the CS frame, the z-axis is defined as the bisector of the angle
 56 between one beam's direction and the opposite direction of the other beam in the rest frame of the
 57 decaying particle. This definition enables the evaluation of polarization parameters with respect to
 58 the motion direction of the colliding hadrons. In the HX reference frame, the z-axis is determined
 59 by the direction of the decaying particle in the center-of-mass frame of the collision. Consequently,
 60 polarization can be assessed with respect to the momentum direction of the J/ψ itself. The y-axis is
 61 perpendicular to the xz-plane (production plane) containing the momenta of the colliding beams and
 62 the decaying particle itself. J/ψ is considered fully transversely or longitudinally polarized when
 63 the polarization parameters take the values of $(\lambda_\theta, \lambda_\phi, \lambda_{\theta\phi}) = (1, 0, 0)$ or $(-1, 0, 0)$, respectively.
 64 No polarization means $(0, 0, 0)$. While the measured polarization values depend on the selection
 65 of the quantization axis, one can construct a frame-invariant quantity to check the consistency of
 66 measurements in different frames. It is defined as

$$\lambda_{inv} = \frac{\lambda_\theta + 3\lambda_\phi}{1 - \lambda_\phi} \quad (2)$$

67 The measurement of λ_{inv} in both the HX and CS frames should give the same value.

68 In the EP frame, the z-axis is chosen to be the direction of global orbital angular momentum
 69 of the system, which is perpendicular to the reaction plane that is estimated by the event plane in
 70 the center of the mass frame of two colliding beams. In the analysis, we use the second-order event
 71 plane based on tracks in the STAR Time Projection Chamber (TPC) as a proxy for the reaction plane
 72 following the same procedure as in the previous study of the STAR Collaboration [14]. Electron
 73 candidates were excluded from the event plane determination, to avoid self-correlation between the
 74 event plane and those J/ψ 's under study.

75 By relating the polarization parameters λ_θ and the spin density matrix element ρ_{00} (Eq.3), the
 76 function describing the angular distribution of the decayed positron in terms of ρ_{00} can be obtained.
 77 The absence of J/ψ spin alignment means that the ρ_{00} is equal to 1/3, while deviation from 1/3
 78 implies the presence of spin alignment.

$$\lambda_\theta = \frac{1 - 3\rho_{00}}{1 + \rho_{00}}, \quad (3)$$

79

$$\frac{dN}{d\cos\theta^*} \propto (1 + \rho_{00}) + (1 - 3\rho_{00})\cos^2\theta^*, \quad (4)$$

80 where θ^* is the polar angle between the z-axis in the EP frame and the momentum direction of the
81 decayed particle. By fitting the angular distribution of decay particles with the function given in
82 Eq.4, one can infer the ρ_{00} value.

83 3. Analysis details

84 3.1 Signal extraction

85 The data used for this analysis is obtained from the STAR detector, which provides a coverage
86 range of $|\eta| < 1$ within the full azimuthal angle ($-\pi < \phi < \pi$). The main subdetectors used in this
87 analysis include TPC, Time-of-Flight (TOF), and Barrel Electromagnetic Calorimeter (BEMC),
88 which are used for electron identification. Data were collected by the STAR detector during the
89 2018 RHIC Ru+Ru and Zr+Zr (isobar) run at a collision energy of $\sqrt{s_{\text{NN}}} = 200$ GeV. The minimum
90 bias (MB) trigger, which is given by a coincidence of signals from the two Zero Degree Calorimeters
91 (ZDCs), is used to select events for our analysis. The electron candidates with opposite-sign charges
92 are paired, and the resulting distribution of invariant mass is depicted in Fig.1. In order to extract
93 the raw J/ψ yield, we perform a fitting procedure on the invariant mass distribution. This fitting
94 procedure involves using a crystal ball function to characterize the J/ψ signal, a mix-event unlike-
95 sign to account for the combinatorial background, and an exponential function to describe the
96 residual background. The parameters of the crystal ball function, including the mean, n , α , and σ ,
97 are fixed to the parameters extracted from the simulation. In the case of J/ψ spin alignment, the
98 yields are derived by extracting J/ψ signal in seven bins of $\cos\theta$ spanning from -1 to 1, within each
99 $p_{\text{T}}^{J/\psi}$ and centrality interval. And, for J/ψ polarization, the yields are obtained through extracting
100 data in ten bins of $\cos\theta$ spanning from -1 to 1 and fifteen bins of ϕ spanning from $-\pi$ to π within
101 each $p_{\text{T}}^{J/\psi}$ and centrality interval. J/ψ yields with a significance less than 3 are disregarded. The
102 upper panels of Fig.2 depict the raw J/ψ yield, represented by black open circles, as a function of
103 $\cos\theta$ and ϕ for a range of $p_{\text{T}}^{J/\psi}$ from 0.2 to 10.0 GeV/c and centrality from 0 to 80% in the CS
104 frame.

105 3.2 Acceptance and efficiency

106 The efficiencies of single electron identification with the TPC and TOF detectors are determined
107 by analyzing a pure electron sample data originating from photon conversions [15]. The TPC
108 tracking efficiency and the efficiency of the electron identification using the BEMC detector are
109 calculated using the embedding technique. The J/ψ acceptance and efficiency ($A \times \epsilon$) as a function
110 of $\cos\theta$ or ϕ is evaluated by folding the single electron and positron efficiency through Monte Carlo
111 (MC) simulations.

112 However, the true distribution of J/ψ decayed positron in MC is not known a priori. The
113 simulation data lack polarization information, potentially resulting in inaccurate efficiency and
114 acceptance values. To address this issue, an iterative procedure for the $A \times \epsilon$ correction is employed,
115 which tunes the J/ψ polarization in the simulation according to data. In the first iteration, the A
116 $\times \epsilon$ is evaluated using non-polarized J/ψ in the simulation, and the polarization parameters are
117 extracted from data after correcting for $A \times \epsilon$. In subsequent iterations, the inputs to the simulation
118 are generated using the polarization parameters acquired from the previous iteration, and the new

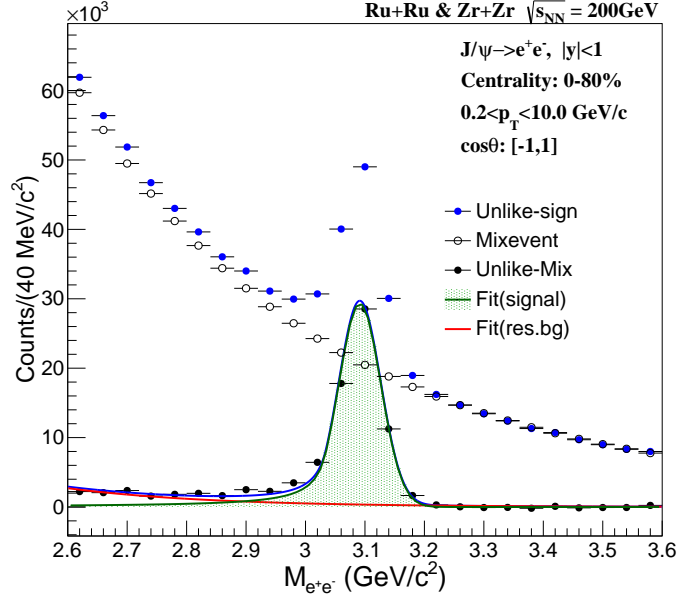


Figure 1: The $e^- e^+$ invariant mass spectrum for the same event unlike-sign (blue solid circles) and mix-event unlike-sign (black open circles) in Ru+Ru and Zr+Zr collisions at $\sqrt{s_{NN}} = 200$ GeV. The black open circles are plotted along with a fit using a crystal ball function (shades of green) for J/ψ signal and an exponential function (red solid line) for the background.

119 polarization parameters are extracted. This process continues until the difference in polarization
 120 parameters between two adjacent iterations is less than 0.1 of the polarization parameter error,
 121 which can be judged as convergence [5].

122 3.3 Extraction of polarization parameters

123 Following the iterative procedure, the efficiency multiplied by the detector acceptance from
 124 the last iteration is shown in the upper panel of Fig.2 as blue dashed lines. These lines are scaled
 125 to have the same integral as the normalized data distribution. To extract the J/ψ polarization in
 126 the dielectron decay channel, we can integrate Eq.1 over ϕ and $\cos\theta$, yielding two one-dimensional
 127 (1D) distributions:

$$W(\cos\theta) \propto 1 + \lambda_\theta \cos^2\theta, \quad (5)$$

128

$$W(\phi) \propto 1 + \frac{2\lambda_\phi}{3 + \lambda_\theta} \cos 2\phi, \quad (6)$$

129 J/ψ polarization parameters (λ_θ and λ_ϕ) can be extracted by simultaneously fitting the cor-
 130 rected yield distributions using Eqs.5 and 6. The lower panels of Fig.2 display the fully corrected
 131 J/ψ yield as a function of $\cos\theta$ and ϕ , along with the simultaneous fit to both distributions repre-
 132 sented by red solid lines. The polarization parameters are obtained from the simultaneous fit and
 133 are listed in Fig.2. Similarly, the J/ψ yield in $|\cos(\theta^*)|$ bins are fitted with Eq.4 to obtain ρ_{00} .

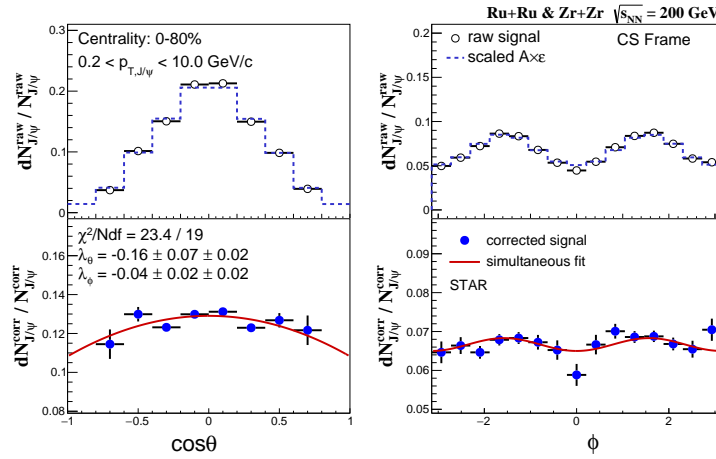


Figure 2: Upper: the raw J/ψ yield and $A \times \epsilon$ as a function of $\cos\theta$ (left) and ϕ (right) from the final iteration of the correction procedure for efficiency and acceptance in the CS frame for $0.2 < p_T^{J/\psi} < 10$ GeV/c. Lower: the acceptance and efficiency corrected J/ψ yields along with the simultaneous fit of corrected yield distributions in $\cos\theta$ and ϕ . The counts are after arbitrary normalization.

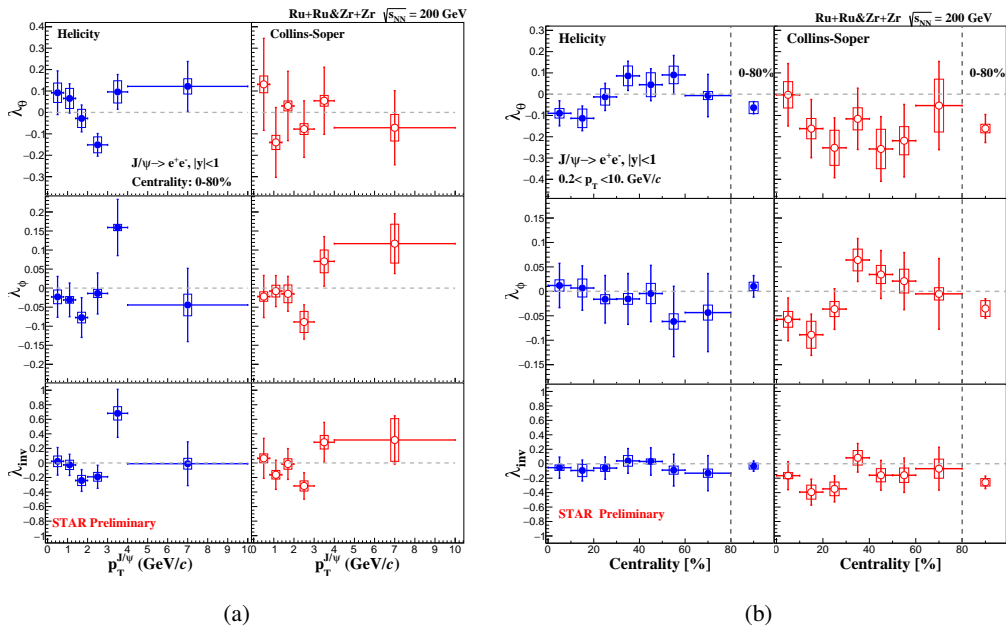


Figure 3: Inclusive J/ψ polarization parameters (from top to bottom: $\lambda_\theta, \lambda_\phi, \lambda_{inv}$) as a function of p_T (a) and centrality (b), with the centrality integrated point shown on the right from the vertical dashed line, for isobaric collisions at $\sqrt{s_{NN}} = 200$ GeV. The error bars indicate statistical uncertainties, while the boxes denote systematic uncertainties. On the left side of the plot, the polarization parameters in the helicity reference frame are presented, while on the right side, those corresponding to the Collins-Soper frame are depicted.

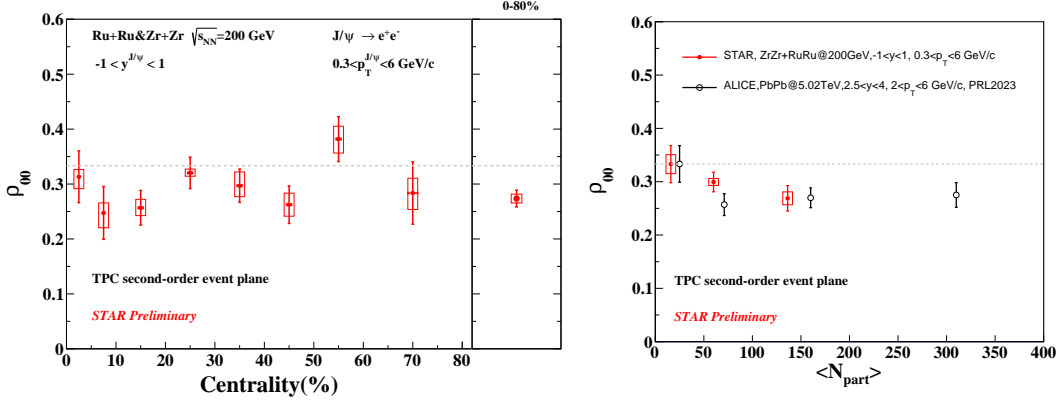


Figure 4: The spin alignment (ρ_{00}) of inclusive J/ψ as a function of centrality (left) and N_{part} (right) for isobar collisions at $\sqrt{s_{NN}} = 200$ GeV in the rapidity interval $-1 < y < 1$, compared with results obtained in Pb + Pb collisions by ALICE at $\sqrt{s_{NN}} = 5.02$ TeV in the rapidity interval $2.5 < y < 4.2$. The statistical uncertainties are represented by vertical bars, while systematic uncertainties are depicted as shaded boxes.

134 4. Results

135 4.1 J/ψ polarization

136 These parameters are measured in six p_T bins, as presented in the left panel of Fig.3. λ_θ and
 137 λ_ϕ are found to be consistent with zero in both the HX and CS frames. There is an indication of
 138 non-trivial p_T dependence observed in the HX frame. The values of λ_{inv} are consistent between
 139 the HX and CS frames. This result is in good agreement, within the uncertainties, with the STAR
 140 measurement in $p+p$ collisions at $\sqrt{s_{NN}} = 200$ GeV [5]. There is no significant dependence of λ_θ
 141 and λ_ϕ observed as the collision centrality varies from central to peripheral events.

142 4.2 J/ψ spin alignment

143 The J/ψ spin alignment (ρ_{00}) in the second-order event plane frame is studied as a function of
 144 centrality and N_{part} in the range of $0.3 < p_T < 6.0$ GeV/c. The results are presented in Fig.4. It is
 145 found that ρ_{00} is lower than $1/3$ with a significance of 3.5σ for p_T ranging from $0.3 < p_T < 6.0$
 146 GeV/c and for events spanning 0-80% centrality. No significant dependence on centrality and N_{part}
 147 is observed within the uncertainties. Interestingly, the value of ρ_{00} at RHIC energy is comparable to
 148 the results obtained at the LHC energy [13] within the uncertainties, despite the different collision
 149 energy, systems, and rapidity.

150 5. Summary

151 We have presented the first measurements of the inclusive J/ψ polarization in HX and CS
 152 frames and spin alignment with respect to the second-order event plane in Ru+Ru and Zr+Zr
 153 collisions at $\sqrt{s_{NN}} = 200$ GeV. The J/ψ polarization parameters are consistent with zero in the p_T
 154 range of 0.2 to 10 GeV/c and centrality range of 0-80% for both the HX and CS frames. Additionally,
 155 no significant centrality or p_T dependence is observed. The λ_{inv} measured in the HX and CS frames
 156 are consistent with each other within uncertainties. J/ψ global spin alignment ρ_{00} is found to be

157 lower than $1/3$ with a significance of 3.5σ for p_T ranging from 0.3 to 6 GeV/ c and centrality
158 range of 0-80%. Moreover, no significant centrality and N_{part} dependence is observed within the
159 uncertainties. The ρ_{00} values at RHIC and LHC energies are similar, despite very different collision
160 energies, systems, and rapidity. Theory calculations are needed to explore the underlying physics.

161 **Acknowledgements**

162 The authors are supported by the National Natural Science Foundation of China under No.
163 11890710, 11890713, and 12105155 and by the Natural Science Foundation of Shandong Province
164 of China with Grant No. ZR2020QA086.

165 **References**

- 166 [1] J.Zhao and B.Chen, arXiv:2312.01799 [hep-ph] 2023
- 167 [2] Z. Liang and X. Wang, Phys. Lett. B **629**, 20 (2005)
- 168 [3] STAR Collaboration, Nature **614**, 244-248 (2023)
- 169 [4] B. Ioffe and D. Kharzeev, Phys. Rev. D **68**, 061902(R) (2003)
- 170 [5] STAR Collaboration, Phys. Rev. D **102**, 092009 (2020)
- 171 [6] P. Faccioli et al, Eur. Phys. J. C **69**: 657-673 (2010)
- 172 [7] ALICE Collaboration, Phys. Rev. Lett. **108**, 082001 (2012)
- 173 [8] ALICE Collaboration, Eur. Phys. J. C **78** (7) (2018)
- 174 [9] LHCb Collaboration, Eur. Phys. J. C **73** (11) 2631 (2013)
- 175 [10] CMS Collaboration, Phys. Lett. B **727** 381–402 (2013)
- 176 [11] ALICE Collaboration, arXiv:2210.08893 [nucl-ex] 2022
- 177 [12] ALICE Collaboration, Phys. Lett. B 815 **815** 136146 (2021)
- 178 [13] ALICE Collaboration, Phys. Rev. Lett. **131** 4, 042303 (2023)
- 179 [14] A. Poskanzer, S. Voloshin, Phys. Rev. C **58**, 1671–1678 (1998).
- 180 [15] PHENIX Collaboration, Phys. Rev. C **81**, 034911 (2010)